Improved Constraints on H_0 from a Combined Analysis of Gravitational-wave and Electromagnetic Emission from GW170817

C. Guidorzi[1] , R. Margutti[2] , D. Brout[3], D. Scolnic[4,11], W. Fong[2,11] , K. D. Alexander[5] , P. S. Cowperthwaite[1] ,
J. Annis[6] , E. Berger[5], P. K. Blanchard[5], R. Chornock[7], D. L. Coppejans[2], T. Eftekhari[5], J. A. Frieman[6,8], D. Huterer[9],
M. Nicholl[5] , M. Soares-Santos[6,10] , G. Terreran[2], V. A. Villar[5] , and P. K. G. Williams[5]

[1] Department of Physics and Earth Science, University of Ferrara, via Saragat 1, I-44122 Ferrara, Italy
[2] Center for Interdisciplinary Exploration and Research in Astrophysics (CIERA) and Department of Physics and Astronomy, Northwestern University, Evanston, IL 60208, USA
[3] Department of Physics and Astronomy, University of Pennsylvania, Philadelphia, PA 19104, USA
[4] Enrico Fermi Institute, Department of Physics, Department of Astronomy and Astrophysics, University of Chicago, Chicago, IL 60637, USA
[5] Harvard-Smithsonian Center for Astrophysics, 60 Garden Street, Cambridge, MA 02138, USA
[6] Fermi National Accelerator Laboratory, P.O. Box 500, Batavia, IL 60510, USA
[7] Astrophysical Institute, Department of Physics and Astronomy, 251B Clippinger Lab, Ohio University, Athens, OH 45701, USA
[8] Department of Astronomy and Astrophysics, University of Chicago, Chicago, IL 60637, USA
[9] Department of Physics, University of Michigan, 450 Church Street, Ann Arbor, MI 48109, USA
[10] Department of Physics, Brandeis University, Waltham, MA 02454, USA

Abstract

The luminosity distance measurement of GW170817 derived from gravitational-wave analysis in Abbott et al. (2017a, hereafter A17:H0) is highly correlated with the measured inclination of the NS–NS system. To improve the precision of the distance measurement, we attempt to constrain the inclination by modeling the broadband X-ray-to-radio emission from GW170817, which is dominated by the interaction of the jet with the environment. We update our previous analysis and we consider the radio and X-ray data obtained at $t < 40$ days since merger. We find that the afterglow emission from GW170817 is consistent with an off-axis relativistic jet with energy $E_k \sim 10^{48} - 3 \times 10^{50}$ erg propagating into an environment with density $n \sim 10^{-2}$–10^{-4} cm^{-3}, with preference for wider jets (opening angle $\theta_j = 15°$). For these jets, our modeling indicates an off-axis angle $\theta_{obs} \sim 25°$–$50°$. We combine our constraints on θ_{obs} with the joint distance–inclination constraint from LIGO. Using the same ~ 170 km s^{-1} peculiar velocity uncertainty assumed in A17:H0 but with an inclination constraint from the afterglow data, we get a value of $H_0 = 74.0 \pm {}^{11.5}_{7.5}$ km s^{-1} Mpc^{-1}, which is higher than the value of $H_0 = 70.0 \pm {}^{12.0}_{8.0}{}_1$ km s^{-1} Mpc^{-1} found in A17:H0. Further, using a more realistic peculiar velocity uncertainty of 250 km s^{-1} derived from previous work, we find $H_0 = 75.5 \pm {}^{11.6}_{9.6}$ km s^{-1} Mpc^{-1} for H_0 from this system. This is in modestly better agreement with the local distance ladder than the Planck cosmic microwave background, though such a significant discrimination will require ~ 50 such events. Measurements at $t > 100$ days of the X-ray and radio emission will lead to tighter constraints.

Key words: gamma-ray burst: general – gravitational waves

1. Introduction

The first gravitational-wave (GW) detection of a binary neutron star (BNS) merger was made on 2017 August 17 at 12:41:02 UT by the Advanced LIGO/Virgo detectors (Abbott et al. 2017b; LIGO Scientific Collaboration & Virgo Collaboration 2017). The event was localized to a region of about 30 deg^2 with an estimated distance of ~ 40 Mpc (LIGO Scientific Collaboration & Virgo Collaboration 2017). A short burst of γ-rays was detected with a delay of about 2 s relative to the merger time by Fermi-GBM and INTEGRAL (Blackburn et al. 2017; Goldstein et al. 2017; Savchenko et al. 2017a, 2017b). Optical follow-up observations of the LIGO/Virgo sky map led to several independent detections of a counterpart, associated with the galaxy NGC 4993 (Arcavi et al. 2017; Coulter et al. 2017; Lipunov et al. 2017; Soares-Santos et al. 2017; Tanvir et al. 2017; Valenti et al. 2017).

It has long been argued that the combination of a distance measurement from a gravitational-wave signal with a redshift measurement from an electromagnetic counterpart can be used to measure cosmological parameters in a novel way, in particular the Hubble constant (Schutz 1986; Holz & Hughes 2005; Dalal et al. 2006). Here, the ratio of the redshift velocity, $v = cz$, of the host galaxy to the absolute distance from the GW event directly yields the Hubble constant such that, for a small redshift z, $v = H_0 \times d$, where v is in km s^{-1}, H_0 is in km s^{-1} Mpc^{-1}, and d is in Mpc. This method has been discussed in Nissanke et al. (2013) and Taylor et al. (2012), which show that with large numbers (20–50) of similar GW–EM detections out to $z \sim 0.1$, percent-level H_0 measurements can be determined. This measurement is important as there is currently 3.4σ tension between the local measurement of H_0 (Riess et al. 2016) and the cosmic microwave background (CMB) measurement of H_0 (Planck Collaboration et al. 2016). The tension may be a hint of new cosmological physics, so independent measurements of H_0 are needed to resolve this issue.

The first BNS event discovered by LIGO–Virgo allows for the first independent measurement of the Hubble constant using GWs (Abbott et al. 2017a, hereafter A17:H0). While previous studies are correct in finding that a number of events are needed to make a percent-level measurement, the current tension in H_0

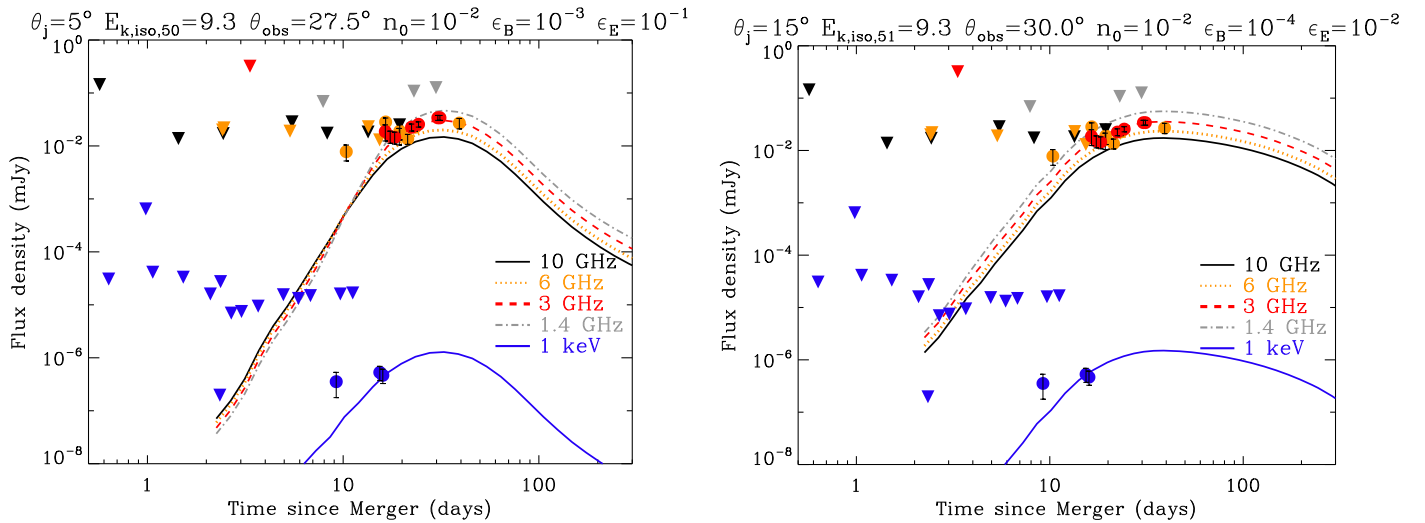**Figure 1.** Off-axis jet models with $\theta_j = 5°$ (left) and $\theta_j = 15°$ (right) that best fit the current set of X-ray (1 keV; blue) and radio observations (black, orange, red, and gray for flux densities at $\sim$10 GHz, $\sim$6 GHz, $\sim$3 GHz, and $\sim$1.4 GHz , respectively). The values of the other model parameters are listed in the plot titles (both have $p = 2.1$). Triangles identify upper limits. These plots show the current data set and demonstrate that the emission from an off-axis relativistic uniform jet can reasonably account for the X-ray and radio observations of GW170817. Wider jets are currently favored by observations because of the milder rise and broader peak of the associated emission, as we found in A17 and M17, and as independently found by Haggard et al. (2017), Hallinan et al. (2017), and Troja et al. (2017). Radio data at 6 GHz are displayed here for comparison, but they have not been used in our calculations (see the text for details).

measurements is large enough that even single GW events could provide interesting constraints. However, the key limitation in the precision of the GW H_0 measurement by A17:H0 is due to the degeneracy between the distance, which is $\sim$40 Mpc, and the orbital inclination angle of the BNS. In this context, the inclination is defined as the angle between the line of sight from source to Earth and the angular momentum of the binary system.

The analysis of the electromagnetic emission from BNS mergers provides an independent constraint on the inclination angle, as these systems are expected to launch relativistic jets aligned with their angular momentum vector (e.g., Eichler et al. 1989; Narayan et al. 1992). The interaction of a relativistic jet with material in the circumbinary environment is a well-known source of non-thermal synchrotron emission across the electromagnetic spectrum (e.g., Sari et al. 1998, 1999; Sari & Piran 1999; Granot & Sari 2002), known as "afterglow" in the gamma-ray burst (GRB) literature. While the UV-optical-NIR emission from a BNS merger can be dominated by the "kilonova" (hereafter KN, i.e., a transient powered by the radioactive decay of r-process nuclei synthesized in the neutron-rich merger ejecta; Metzger 2017), the jet interaction with the circumbinary medium dominates the X-ray and radio portion of the electromagnetic spectrum, with observable properties that directly depend on the binary inclination angle with respect to the line of sight (e.g., Granot et al. 2002; Rossi et al. 2002).

In this Letter, we build on our previous analysis of the X-ray and radio emission from GW170817 (Alexander et al. 2017, hereafter A17; Margutti et al. 2017, hereafter M17). We update our modeling to include all the available data obtained at $t < 40$ days since NS–NS coalescence, and we run a more extended and finer grid of off-axis jets simulations. Our data set is described in Section 2, while in Section 3 we employ realistic models of synchrotron emission from off-axis relativistic jets to estimate the BNS jet parameters. We combine the estimate of the binary inclination angle obtained with these models with the GW measurement and improve the distance determination

of GW170817 in Section 4. We conclude in Section 5. With this pilot study we demonstrate that the combination of GW and EM observations of the *same* BNS merger improves the accuracy of the measurement of cosmological parameters.

In this Letter, we list 1σ c.l. uncertainties unless otherwise stated and employ the notation $Q_x \equiv Q/10^x$.

2. Data Set

We collected the available X-ray and radio observations of GW170817 acquired at $t < 40$ days since merger (Figure 1). This data set includes Karl G. Jansky Very Large Array (VLA) observations at different frequencies ($\sim$10 GHz, 6 GHz, 3 GHz, and 1.4 GHz) and X-ray observations with the *Chandra* X-ray Observatory (CXO). The original data sets have been published in A17, M17, Haggard et al. (2017), Hallinan et al. (2017), Kim et al. (2017), and Troja et al. (2017). We refer to these papers for details about data acquisition and reduction. For internal consistency, we cross-calibrated the X-ray observation from Troja et al. (2017) using the published count-rate of 12 photons in 50 ks of CXO observations with the spectral parameters of M17. Additionally, given the larger degree of uncertainty affecting the flux calibration of radio observations acquired at 6 GHz (Hallinan et al. 2017), we concentrate our modeling on the 1.4 GHz, 3 GHz, and 10 GHz data sets. The entire data set, inclusive of the 6 GHz data points, is shown in Figure 1.

For the measurement of H_0, we follow A17:H0 and use the heliocentric recessional velocity of 2995 km s^{-1} from Kourkchi & Tully (2017), as NGC 4993 can be associated as part of the group ESO-508. Applying a bulk flow estimate from 2M++ of -300 km s^{-1} to the redshift in the velocity in the CMB frame, they find a final velocity of 3017 km s^{-1}. The uncertainty for the redshift from A17:H0 is 150 km s^{-1}. This redshift and uncertainty are analyzed in Hjorth et al. (2017), which find a lower mean heliocentric velocity of the group and a final velocity of 2922 km s^{-1}. The magnitude of the peculiar velocity uncertainty is reconsidered below, and the shift from Hjorth et al. (2017) is also propagated as a variant in the analysis.

3. Modeling of the Broadband Afterglow Emission

There are four main potential contributions to the X-ray and radio flux observed with GW170817 that must be considered to properly model the afterglow emission: (1) synchrotron emission from the interstellar medium (ISM) shocked by the KN ejecta, (2) central engine long-lasting activity, (3) emission from mildly relativistic ejecta that are expected off-axis (e.g., from a cocoon), and (4) synchrotron emission from the ISM shocked by a relativistic off-axis jet. The contribution of (1) is negligible at both X-ray and radio wavelengths in the time span considered here because the associated sub-relativistic ($v/c \sim$ 0.1–0.3), slowly decelerating outflow of the large ejecta mass ($0.01 - 0.1\,M_\odot$) that is estimated for GW170817 (Arcavi et al. 2017; Chornock et al. 2017; McCully et al. 2017; Nicholl et al. 2017; Pian et al. 2017; Shappee et al. 2017; Smartt et al. 2017) is expected to take over much later and finally peak in the radio after several years (A17 and references therein). The possible contribution of (2) cannot account for the observed X-ray flux because this would be suppressed by the huge bound-free opacity of the r-process heavy elements in the KN ejecta (see M17 and references therein), while the radio flux would equally be free–free absorbed. While the cocoon model (3) is not ruled out, the electron energy distribution inferred from the radio+ X-ray data modeling discussed in M17 and in A17 is better described by a shallow power-law (index $p \sim 2.1$), which leans toward the interpretation of synchrotron radiation from an off-axis jet (4). Here, we proceed under the same hypothesis (4). When modeling the afterglow emission with this interpretation, we do not include the optical data because the corresponding flux is dominated by the KN contribution and its subtraction would be critically dependent on its modeling (Cowperthwaite et al. 2017; Drout et al. 2017; Smartt et al. 2017; Tanvir et al. 2017).

We calculated a multi-wavelength set of light curves with the publicly available code BOXFIT (v2; van Eerten et al. 2010; van Eerten & MacFadyen 2012), which assumes a uniform jet with kinetic energy E_k plowing through a constant interstellar medium with density n. By varying E_k, n, p (power-law index of the electron energy distribution), ϵ_B, ϵ_e (fraction of post-shock energy in magnetic fields and electrons, respectively), and θ_j (jet opening angle), we calculate the off-axis afterglow emission as observed from different lines of sight θ_{obs}, with θ_{obs} varying from $\theta_j + \delta\theta$ to $90°$ (i.e., equatorial view) with a fixed pace of $\delta\theta = 2.5°$. In this Letter, we always refer to isotropic-equivalent luminosities, but we differentiate between isotropic-equivalent kinetic energy $E_{k,iso}$ and beaming-corrected kinetic energy of the blast wave E_k, where $E_k = E_{k,iso}(1 - \cos\theta_j)$.

We explore a wide portion of parameter space corresponding to $E_{k,iso} = 3 \times 10^{49}$ –3×10^{52} erg, $n = 10^{-4}$–$1\,\mathrm{cm}^{-3}$, $\epsilon_B = 10^{-4}$–10^{-1}, and $\epsilon_e = 0.01$–0.1. These ranges were chosen so as to cover the observed distributions for the short GRB sample by Fong et al. (2015). We did not consider extremely low density environments ($n < 10^{-4}\,\mathrm{cm}^{-3}$), as these were observed in conjunction with very large offsets from the host centers ($\gtrsim 10\,r_e$), whereas this is merely $0.64\,r_e$ for GRB 170817A (Blanchard et al. 2017; Fong et al. 2017). Except for θ_{obs}, the grid is logarithmically paced as in Table 1. We a priori excluded all $\theta_{obs} \leqslant \theta_j$ cases as clearly incompatible with the initially rising X-ray afterglow peaking at $\geqslant 15$ days (M17). We explored two values of the power-law index of the electron distribution $p = 2.1$ and $p = 2.2$ (as expected from particle

Table 1
Parameters of Off-axis Jet Simulations with BOXFIT

Parameter	Range of Values	Grid Pace
Jet Isotropic Energy $E_{k,iso}$ (erg)	3×10^{49}–3×10^{52}	0.5 dec
Circum-merger density n (cm^{-3})	10^{-4}–1	0.5 dec
Observer angle θ_{obs} (deg)	$(\theta_j + 2.5)$–90	2.5
ϵ_B	10^{-4}–10^{-1}	1 dec
ϵ_e	0.01–0.1	1 dec
p	2.1–2.2	0.1

Note. Simulations were run at two fixed values of jet opening angles $\theta_j = 5°$ and $\theta_j = 15°$, propagating in a constant density medium.

acceleration in the ultra-relativistic limit; Sironi et al. 2015). Current X-ray and radio observations favor $p = 2.1$. We do not consider values $p > 2.2$ (such as $p = 2.4$, median value from short GRBs afterglows from Fong et al. 2015) for the reasons we already discussed in M17 and A17. We run each simulation for a collimated $\theta_j = 5°$ jet and a jet with $\theta_j = 15°$, representative of a less collimated outflow. Our choice encompasses the bulk of the distribution of estimated θ_j's for short GRBs (Fong et al. 2015 and references therein).

To usefully limit the number of grid points in the parameter space, we preliminarily impose two observationally driven constraints: (i) the peak time of the afterglow, calculated as $t_p = 2.1\,E_{k,iso,52}^{1/3}\,n_0^{-1/3}((\theta_{obs} - \theta_j)/10°)^{8/3}$ days (Granot et al. 2002), must lie in the range $10 < t_p < 300$ days ($E_{k,iso,52} = E_{k,iso}/10^{52}$ erg; $n_0 = n/1\,\mathrm{cm}^{-3}$); and (ii) the flux density at 1 keV at $t \sim t_p$, calculated as $F_\nu(t_p) \propto \epsilon_e^{p-1}\,\epsilon_B^{(p+1)/4}\,n^{(p+1)/4}\,E_{k,iso}(\theta_{obs} - \theta_j)^{2(1-p)}$ (assuming X-rays lie between synchrotron peak and cooling frequency, in the slow cooling regime, as expected at this epoch; e.g., Granot & Sari 2002), must match the observed flux at 15 days within a factor of ~ 30.

The final multi-parameter posterior is estimated from the combination of a likelihood function that assigns each model m_i a probability $p_i \propto \exp(-\chi_i^2/2)$, with χ_i^2 evaluated from comparing m_i with the entire broadband set of data and upper limits, along with an uninformative, scale-invariant prior on each logarithmically paced parameter. Such a prior is flat on logarithms. The final marginalized posterior on the only interesting parameter θ_{obs} is obtained by approximating the integration of the posterior over the remaining nuisance parameter space as a sum over all of the grid points. This way, the scale-invariant prior is automatically encoded, as a logarithmically paced grid is equivalent to a flat distribution on logarithms.

Overall, we confirm the results that we published in M17 and A17. The mild temporal evolution of the X-ray and radio emission favors wider jet opening angles $\theta_j = 15°$ (similar θ_j are invoked by Hallinan et al. 2017 and Troja et al. 2017 in their analysis). For $\theta_j = 15°$, our simulations favor $n \sim 10^{-4}$–$10^{-2}\,\mathrm{cm}^{-3}$, 10^{48} erg $< E_k \leqslant 3 \times 10^{50}$ erg, and $\theta_{obs} \sim 25°$–$50°$. For both jet opening angles, the measurement of θ_{obs} is degenerate with n and E_k, with larger E_k/n fractions favoring lower θ_{obs}. We show the posterior probability density function (PDF) of θ_{obs} in Figure 2, smoothed with a Gaussian kernel with $\sigma = 7.5°$ (=$3\,\delta\theta$). These estimates assume a luminosity distance to NGC 4993 $d_L = 39.5$ Mpc as listed in the NASA Extragalactic Database (NED). Varying d_L between 36–43 Mpc (full range of distances reported in NED; Han & Mould 1992; Sakai et al. 2000; Freedman et al. 2001) produces
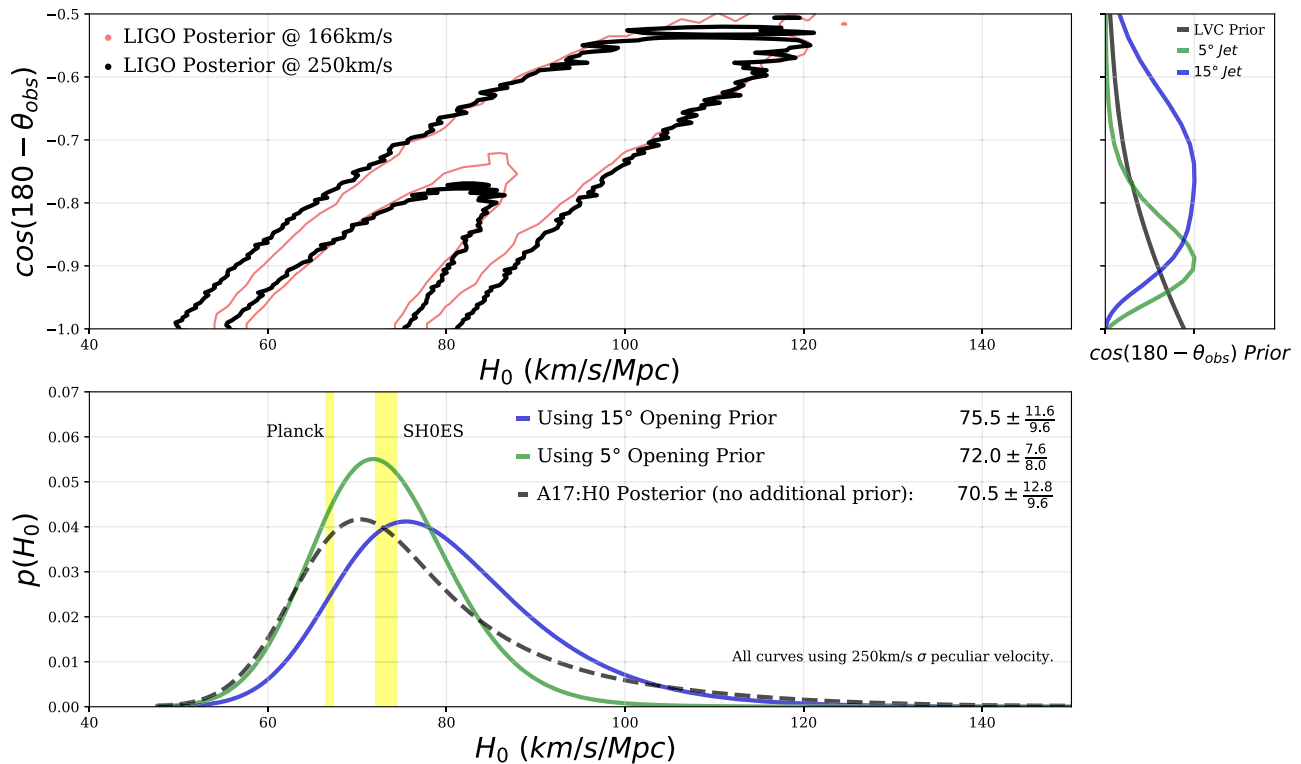
Figure 2. Constraints on the Hubble constant H_0 for GW170817 with and without prior on the inclination of the system. Top: black 1σ and 2σ contours from the LIGO data server assume 166 km s^{-1} peculiar velocity uncertainty. Red 1σ and 2σ contours noised to 250 km s^{-1} peculiar velocity uncertainty. Right: visual representation of the calculated priors on θ_{obs}. Also shown is the marginalized posterior of the A17:H0 data alone. Bottom: marginalized constraints on H_0 for our two scenarios for which inclination priors have been calculated as well as for the noised-up 250 km s^{-1} LIGO contour alone.

negligible impact on our final estimates. Finally, we note that the X-ray (and maybe the 6 GHz) excess at early times ($t < 10$ days; Figure 1) might be the signature of a structured jet (i.e., a jet with energy profile that deviates from uniform and without a sharp edge; e.g., Rossi et al. 2002; Zhang & Mészáros 2002; Kathirgamaraju et al. 2018). Both Gaussian and power-law structured jets would be brighter than uniform jets when viewed from the same θ_{obs} before peak, while having a similar evolution at later times (see, e.g., Troja et al. 2017, their Extended Data Figure 3).

4. Constraints on H_0

4.1. LIGO Data

We use the Markov chains from A17:H0 from the 2D plane of distance and the cosine of inclination angle of the binary star system. This is shown in Figure 2 (top).

4.2. Redshift Uncertainty

Every galaxy responds to the pull of large-scale structure, resulting in the so-called peculiar velocity. The observed velocity is the sum of the Hubble expansion at that redshift and the line-of-sight component of the peculiar velocity, $v_{obs} = v + (v_{pec})_\parallel$. To account for $(v_{pec})_\parallel$, we adopt three alternate approaches. Here, we assume that the uncertainty in the redshift of the group by modeling the individual redshifts is subdominant to the peculiar velocity uncertainties.

First, we follow A17:H0 and correct the redshift by the large-scale bulk flow correction from 2M++ as described in Carrick et al. (2015). The uncertainty of this correction is 150 km s^{-1} for halos, as estimated in N-body simulations from

Carrick et al. (2015), and the uncertainty was increased in A17:H0 by 70 km s^{-1} in quadrature due to additional correction uncertainties. This should be considered a lower floor on the uncertainty because it assumes the ability to convert from galaxy luminosity observations to the total matter field (and thus peculiar velocity) in three dimensions—a process that is subject to systematics because of the uncertainties in how light traces mass.

For a more conservative estimate of the peculiar velocity uncertainty, we can simply estimate the statistical variance in H_0 expected at $z = 0.01$, without attempting to correct for it. We adopt the results from Wu & Huterer (2017), who used a large-volume cosmological N-body simulation to quantify the variance in the local value of H_0 (Riess et al. 2016) due to local density fluctuations and the SN sample selection. We use the largest volume in the public release of the Dark Sky simulations[12] (Skillman et al. 2014), with $10{,}240^3$ particles within a volume of $(8\,h^{-1}\mathrm{Gpc})^3$ ($h = H_0/(100\,\mathrm{km\,s^{-1}\,Mpc^{-1}}$)) and the mass resolution of $3.9 \times 10^{10}\,h^{-1}M_\odot$. We place observers at centers of 512 subvolumes of $(1\,h^{-1}\mathrm{Gpc})^3$; in each subvolume, we identify all halos in the virial mass range $[10^{12.3}, 10^{12.4}]\,M_\odot$, then further identify the closest-match halos to redshift $z = 0.01$ in random directions on the sky. For each of these closest-match halos and in each subvolume, we measure $dH_0 = (v_{pec})_\parallel/r$. We then calculate the variance of these measurements, $\sigma^2((v_{pec})_\parallel)$, which corresponds to the expected range due to peculiar velocity for an object at $z = 0.01$ observed anywhere in the universe. The corresponding rms is $\sigma((v_{pec})_\parallel) \approx 260$ km s^{-1}, and it is robust with

---

[12] http://darksky.slac.stanford.edu

respect to simulation statistics as well as the choice of the halo mass range.

A compromise is to apply the bulk flow corrections, but include a more conservative estimate of the peculiar velocity uncertainty as done in Scolnic et al. (2017a), which compares the dispersion in SNIa distance residuals for $z \sim 0.01$ SNe and $z \sim 0.05$ SNe after bulk flow corrections are applied. The main difference in the dispersion is the impact of the peculiar velocities, which is determined to be 250 km s^{-1} (and 270 km s^{-1} if bulk flows were not applied). Since there is consistency between this estimate of the uncertainty and that derived based on the Wu & Huterer (2017) analysis above, we adopt 250 km s^{-1}. Furthermore, this estimate is consistent with the uncertainty estimated in Hjorth et al. (2017) of 232 km s^{-1}. This uncertainty is $\sim 8\%$ of the galaxy velocity.

We show the inclination versus H_0 posterior for a peculiar velocity uncertainty of 166 and 250 km s^{-1} in Figure 2 (top). We find a small shift in the contours due to edge effects as well as the smoothing of the posterior with an additional velocity uncertainty.

4.3. Inclination Priors from EM Data Modeling

Broadband X-ray-to-radio observations provide an independent measurement of the inclination of the BNS system, which we quantified in Section 3 in terms of θ_{obs}. NS–NS mergers are expected to launch two jets in opposite directions. θ_{obs} is the angle between the observer's line of sight and the closest of the two jets. For this system, the inclination angle is $i = 180° - \theta_{obs}$. We reanalyze the LIGO posteriors incorporating the θ_{obs} constraints obtained from the X-ray and radio afterglow modeling to produce an updated estimate of H_0 (Section 4.4).

As a refinement, we consider additional constraints on θ_{obs} derived from modeling of the optical and near-infrared light curves and spectra of GW170817 (Chornock et al. 2017; Cowperthwaite et al. 2017; Díaz et al. 2017; Kilpatrick et al. 2017; McCully et al. 2017; Nicholl et al. 2017; Pian et al. 2017; Tanaka et al. 2017; Tanvir et al. 2017; Valenti et al. 2017). Explaining the observed emission requires the inclusion of an early-time "blue" kilonova component, consistent with lanthanide-poor ejecta, which implies $\theta_{obs} \lesssim 45°$ (Kasen et al. 2015; Sekiguchi et al. 2016; Metzger 2017), in agreement with the low degree of measured linear optical polarization (Covino et al. 2017). For $\theta_{obs} \gg 45°$ the blue kilonova emission would be obscured by the lanthanide-rich (and thus high opacity) dynamical ejecta in the equatorial plane. We note, however, that this interpretation is more model-dependent and makes assumptions about the ejecta geometry. For example, this interpretation would not be necessarily true if instead the blue emission is almost always visible due to the lanthanide-poor material having a higher expansion velocity compared to the lanthanide-rich material.

4.4. Results

Our recovered estimates of H_0 are summarized in Table 2. We present a series of variations in our analysis based on the different priors from inclination and the different uncertainties on the peculiar velocity. It is notable that in almost all of our variations, the overall best-fit value of H_0 is higher than in A17:H0. This is due to the higher inclination angle favored in our modeling. The increase in H_0 pushes our result away from Planck Collaboration et al. (2016) and toward the value

Table 2
Results

#	Priors (km s^{-1})	$\sigma_{\rm vpec}$ (km s^{-1} Mpc^{-1})	H_0
1	Baseline (15° Jet Width)	250	$75.5 \pm \frac{11.6}{9.6}$
2	15° Jet Width, v = 2922 km s^{-1a}	250	$73.1 \pm \frac{11.3}{9.3}$
3	15° Jet Width	166	$74.0 \pm \frac{11.5}{7.5}$
4	5° Jet Width	250	$72.0 \pm \frac{7.6}{8.0}$
5	5° Jet Width	166	$71.0 \pm \frac{7.1}{5.7}$
6	$\theta_{obs} < 45°$ (KN)	250	$70.5 \pm \frac{12.7}{8.9}$
7	None	250	$70.5 \pm \frac{12.8}{9.6}$
8	None	166	$69.4 \pm \frac{12.0}{7.7}$

Note. Values reported for H_0 are maximum a posteriori intervals (smallest range enclosing 68% of the posterior).
[a] Denotes heliocentric velocity obtained from Hjorth et al. (2017) of 2922 km s^{-1}. All other values reported use A17:H0 velocity estimate of 3017 km s^{-1}.

measured by the SH0ES collaboration (Riess et al. 2016), though for our baseline case with a 15° jet angle and 250 km s^{-1}, Planck Collaboration et al. (2016) is only disfavored at $\sim 1\sigma$.

We also include a shifted best-fit value of H_0 using the final velocity modeled in Hjorth et al. (2017). We performed an independent verification of their velocity estimate using the AAOmega spectrograph (Smith et al. 2004; Sharp et al. 2006), in which we obtained redshifts of 24 galaxies in the group and calculated a mean heliocentric recessional velocity of 2953 km s^{-1}. Using the peculiar velocity correction from Carrick et al. (2015) we find a velocity of 2939 km s^{-1} in the CMB frame. Our independent estimate agrees more with Hjorth et al. (2017) than that of A17:H0, and therefore we use Hjorth et al. (2017) as a variant in this analysis. In this scenario, H_0 decreases by $\sim 3\%$, but a robust calculation requires a complex shift of the chains provide in A17:H0. As a further test, we investigated the robustness of our H_0 estimates against the choice of scale-invariant priors on the afterglow parameters, trying with arbitrary priors that favor combinations of large $E_{k,\rm iso}$ and low n. Even though this possibility is unsupported by current prior information from available samples such as that by Fong et al. (2015), the consequent best values and uncertainty intervals on H_0 changed by $\lesssim 2\%$ and by $\lesssim 15\%$, respectively, leaving the results discussed above essentially unaffected.

5. Summary and Conclusions

In this study, we combined constraints on the inclination from modeling of the electromagnetic observations of GW170817 with the correlated constraints between distance and inclination as presented in A17:H0. While our inclination constraints from modeling of EM data are model dependent, our best-fit case assuming the favored 15° jet angle yields $H_0 = 75.5 \pm \frac{11.6}{9.6}$ km s^{-1} Mpc^{-1}. If we assume a 5° jet angle, we measure $H_0 = 72.0 \pm \frac{7.6}{8.0}$ km s^{-1} Mpc^{-1}. Both of these measurements are shifted toward higher H_0 values from $H_0 = 70.0 \pm \frac{12.0}{8.0}$ km s^{-1} Mpc^{-1} in A17:H0. Our uncertainty on H_0 for the 15° case is not significantly reduced when applying the inclination constraints, partly due to our increase

in the peculiar velocity uncertainty from A17:H0. Still, it can be noted our recovered H_0 value marginally favors the Riess et al. (2016) over the Planck Collaboration et al. (2016) by $\sim 1\sigma$.
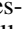
We find that the leverage from the independent inclination measurement reduces to the size of the uncertainty interval on H_0 by $\sim 5\%$: comparing rows 1 and 7 of Table 2 the MAP reduces from 22.4 to 21.2 km s^{-1} Mpc^{-1}. We were very fortunate that this event was so close and provided tighter than expected constraints on H_0. Using the distance–inclination degeneracy resulting from this event we are able to predict the number of events with host galaxy identification needed to perform an H_0 measurement of similar constraints to that of SH0ES: $\sigma = 1.7$ km s^{-1} Mpc^{-1} (Riess et al. 2016). We run a Monte Carlo simulation of BNS events out to 80 Mpc and assume that uncertainties on the distance of an event remain proportional to the distance with the same constant of proportionality to that of event GW170817. We account for the uncertainty in peculiar velocity of each simulated event which is inversely proportional to the event distance. Additionally we have assumed a BNS detection limit of 80 Mpc based on O2 predictions and thus is a conservative estimate for LIGO O3 run. We find that under the aforementioned assumptions, ~ 50 such events using similar X-ray/radio constraints are needed to obtain a constraint on H_0 with a minimum 68% confidence interval of ~ 3.5 km s^{-1} Mpc^{-1}. We look forward to improving these Monte Carlo predictions with improvements to the constraints on the inclination with observations at $t \gtrsim 100$ days since merger, when GW170817 will be observable again in the X-rays.

If GW events are similar to GW170817, it will be possible to detect future GW events at X-ray and radio wavelengths out to a distance of ~ 100 Mpc.[13] Since the inclination constraint from X-ray and radio data gets worse at further distances, but the impact of uncertainties in the peculiar velocities on H_0 is inversely proportional to distance, the overall H_0 uncertainty of future events is likely to be similar to our calculated uncertainty for GW170817. For a very competitive measurement of H_0 from GW events, both the sensitivity of GW detectors as well as X-ray and radio detectors must increase.

ORCID iDs

C. Guidorzi ⓘ https://orcid.org/0000-0001-6869-0835
R. Margutti ⓘ https://orcid.org/0000-0003-4768-7586
W. Fong ⓘ https://orcid.org/0000-0002-7374-935X
K. D. Alexander ⓘ https://orcid.org/0000-0002-8297-2473
P. S. Cowperthwaite ⓘ https://orcid.org/0000-0002-2478-6939
J. Annis ⓘ https://orcid.org/0000-0002-0609-3987
E. Berger ⓘ https://orcid.org/0000-0002-9392-9681
M. Nicholl ⓘ https://orcid.org/0000-0002-2555-3192
M. Soares-Santos ⓘ https://orcid.org/0000-0001-6082-8529
V. A. Villar ⓘ https://orcid.org/0000-0002-5814-4061
P. K. G. Williams ⓘ https://orcid.org/0000-0003-3734-3587

References

Abbott, B. P., Abbott, R., Abbott, T. D., et al. 2017a, Natur, 551, 85
Abbott, B. P., Abbott, R., Abbott, T. D., et al. 2017b, PhRvL, 119, 161101
Alexander, K. D., Berger, E., Fong, W., et al. 2017, ApJL, 848, L21
Arcavi, I., McCully, C., Hosseinzadeh, G., et al. 2017, ApJL, 848, L33
Blackburn, L., Briggs, M. S., Broida, J., et al. 2017, GCN, 21506
Blanchard, P. K., Berger, E., Fong, W., et al. 2017, ApJL, 848, L22
Carrick, J., Turnbull, S. J., Lavaux, G., & Hudson, M. J. 2015, MNRAS, 450, 317
Chornock, R., Berger, E., Kasen, D., et al. 2017, ApJL, 848, L19
Coulter, D. A., Foley, R. J., Kilpatrick, C. D., et al. 2017, Sci, https://doi.org/10.1126/science.aap9811
Covino, S., Wiersema, K., Fan, Y. Z., et al. 2017, NatAs, 1, 791
Cowperthwaite, P. S., Berger, E., Villar, V. A., et al. 2017, ApJL, 848, L17
Dalal, N., Holz, D. E., Hughes, S. A., & Jain, B. 2006, PhRvD, 74, 063006
Díaz, M. C., Macri, L. M., Garcia Lambas, D., et al. 2017, ApJL, 848, L29
Drout, M. R., Piro, A. L., Shappee, B. J., et al. 2017, Sci, https://doi.org/10.1126/science.aaq0049
Eichler, D., Livio, M., Piran, T., & Schramm, D. N. 1989, Natur, 340, 126
Fong, W., Berger, E., Blanchard, P. K., et al. 2017, ApJL, 848, L23
Fong, W., Berger, E., Margutti, R., & Zauderer, B. A. 2015, ApJ, 815, 102
Freedman, W. L., Madore, B. F., Gibson, B. K., et al. 2001, ApJ, 553, 47
Goldstein, A., Veres, P., Burns, E., et al. 2017, ApJL, 848, L14
Granot, J., Panaitescu, A., Kumar, P., & Woosley, S. E. 2002, ApJL, 570, L61
Granot, J., & Sari, R. 2002, ApJ, 568, 820
Haggard, D., Nynka, M., Ruan, J. J., et al. 2017, ApJL, 848, L25
Hallinan, G., Corsi, A., Mooley, K. P., et al. 2017, Sci, https://doi.org/10.1126/science.aap9855
Han, M., & Mould, J. R. 1992, ApJ, 396, 453

---

[13] It will be possible to detect similar systems at $d > 100$ Mpc only if the jet is closer to our line of sight, so likely will not be able to follow the large numbers of KN detections predicted in Scolnic et al. (2017b).

Hjorth, J., Levan, A. J., Tanvir, N. R., et al. 2017, ApJL, 848, L31
Holz, D. E., & Hughes, S. A. 2005, ApJ, 629, 15
Kasen, D., Fernández, R., & Metzger, B. D. 2015, MNRAS, 450, 1777
Kathirgamaraju, A., Barniol Duran, R., & Giannios, D. 2018, MNRAS, 473, L121
Kilpatrick, C. D., Foley, R. J., Kasen, D., et al. 2017, Sci, https://doi.org/10.1126/science.aaq0073
Kim, S., Schulze, S., Resmi, L., et al. 2017, ApJL, 850, L21
Kourkchi, E., & Tully, R. B. 2017, ApJ, 843, 16
LIGO Scientific Collaboration & Virgo Collaboration 2017, GCN, 21509
Lipunov, V. M., Gorbovskoy, E., Kornilov, V. G., et al. 2017, ApJL, 850, L1
Margutti, D., Berger, E., Fong, W., et al. 2017, ApJL, 848, L23
McCully, C., Hiramatsu, D., Howell, D. A., et al. 2017, ApJL, 848, L32
Metzger, B. D. 2017, LRR, 20, 3
Narayan, R., Paczynski, B., & Piran, T. 1992, ApJL, 395, L83
Nicholl, M., Berger, E., Kasen, D., et al. 2017, ApJL, 848, L18
Nissanke, S., Holz, D. E., Dalal, N., et al. 2013, arXiv:1307.2638
Pian, E., D'Avanzo, P., Benetti, S., et al. 2017, Natur, 551, 67
Planck Collaboration, Ade, P. A. R., Aghanim, N., et al. 2016, A&A, 594, A13
Riess, A. G., Macri, L. M., Hoffmann, S. L., et al. 2016, ApJ, 826, 56
Rossi, E., Lazzati, D., & Rees, M. J. 2002, MNRAS, 332, 945
Sakai, S., Mould, J. R., Hughes, S. M. G., et al. 2000, ApJ, 529, 698
Sari, R., & Piran, T. 1999, ApJ, 520, 641
Sari, R., Piran, T., & Halpern, J. P. 1999, ApJL, 519, L17
Sari, R., Piran, T., & Narayan, R. 1998, ApJL, 497, L17
Savchenko, V., Ferrigno, C., Kuulkers, E., et al. 2017a, ApJL, 848, L15

Savchenko, V., Mereghetti, S., Ferrigno, C., et al. 2017b, GCN, 21507
Schutz, B. 1986, Natur, 323, 310
Scolnic, D. M., Jones, D. O., Rest, A., et al. 2017a, ApJ, submitted (arXiv:1710.00845)
Scolnic, D. M., Kessler, R., Brout, D., et al. 2017b, ApJ, submitted (arXiv:1710.05845)
Sekiguchi, Y., Kiuchi, K., Kyutoku, K., Shibata, M., & Taniguchi, K. 2016, PhRvD, 93, 124046
Shappee, B. J., Simon, J. D., Drout, M. R., et al. 2017, Sci, https://doi.org/10.1126/science.aaq0186
Sharp, R., Saunders, W., Smith, G., et al. 2006, Proc. SPIE, 6269, 62690G
Sironi, L., Keshet, U., & Lemoine, M. 2015, SSRv, 191, 519
Skillman, S. W., Warren, M. S., Turk, M. J., et al. 2014, arXiv:1407.2600
Smartt, S. J., Chen, T.-W., Jerkstrand, A., et al. 2017, Natur, 551, 75
Smith, G. A., Saunders, W., Bridges, T., et al. 2004, Proc. SPIE, 5492, 410
Soares-Santos, M., Holz, D. E., Annis, J., et al. 2017, ApJL, 848, L16
Tanaka, M., Utsumi, Y., Mazzali, P. A., et al. 2017, PASJ, 69, 102
Tanvir, N. R., Levan, A. J., González-Fernández, C., et al. 2017, ApJL, 848, L27
Taylor, S. R., Gair, J. R., & Mandel, I. 2012, PhRvD, 85, 023535
Troja, E., Piro, L., van Eerten, H., et al. 2017, Natur, 551, 71
Valenti, S., Sand, D. J., Yang, S., et al. 2017, ApJL, 848, L24
van Eerten, H., Zhang, W., & MacFadyen, A. 2010, ApJ, 722, 235
van Eerten, H. J., & MacFadyen, A. I. 2012, ApJ, 751, 155
Wu, H.-Y., & Huterer, D. 2017, MNRAS, 471, 4946
Zhang, B., & Mészáros, P. 2002, ApJ, 581, 1236